

Climate change impact on waves in the Bay of Biscay, France

Elodie Charles · Déborah Idier · Pascale Delecluse ·
Michel Déqué · Gonéri Le Cozannet

Received: 22 December 2011 / Accepted: 2 March 2012 / Published online: 24 March 2012
© The Author(s) 2012. This article is published with open access at Springerlink.com

Abstract The knowledge of offshore and coastal wave climate evolution towards the end of the twenty-first century is particularly important for human activities in a region such as the Bay of Biscay and the French Atlantic coast. Using dynamical downscaling, a high spatial resolution dataset of wave conditions in the Bay of Biscay is built for three future greenhouse gases emission scenarios. Projected wave heights, periods and directions are analysed at regional scale and more thoroughly at two buoys positions, offshore and along the coast. A general decrease of wave heights is identified (up to -20 cm during summer within the Bay of Biscay), as well as a clockwise shift of summer waves and winter swell coming from direction. The relation between those changes and wind changes is investigated and highlights a complex association of processes at several spatial scales. For instance, the intensification and the northeastward shift of strong wind core in the North Atlantic Ocean explain the clockwise shift of winter swell directions. During summer, the decrease of the westerly winds in the Bay of Biscay explains the clockwise shift and the wave height decrease of

wind sea and intermediate waves. Finally, the analysis reveals that the offshore changes in the wave height and the wave period as well as the clockwise shift in the wave direction continue toward the coast. This wave height decrease result is consistent with other regional projections and would impact the coastal dynamics by reducing the longshore sediment flux.

Keywords Climate change · Wave climate · Dynamical downscaling · Bay of Biscay

1 Introduction

Within the context of climate change, one of the recurrent question is how this change could impact waves and thus wave-dominated coasts. As an example, the Bay of Biscay is bounded by the coast from Brittany (France) to Galicia (Spain). French Western coast and Spanish Northern coast are both characterized by intense human activity: sea transport, fishing, coastal shipping, ports, seaside resorts, touristic sandy beaches and surfing areas. Since the Bay of Biscay is largely open to the ocean, its wave climate is characterized by swells and storms generated by strong winds in the North Atlantic Ocean. A change in these wave conditions could modify the coastal morphology (e.g. Thiébot et al. 2011) and impact the human activity.

In the context of global warming, significant climate changes at the oceanic basin scale could modify the wave climate. General circulation models (GCM) indeed project atmospheric changes such as a poleward shift of storm tracks (Yin 2005) or a decrease of the total number and intensity of cyclones in the Northern Hemisphere (Catto et al. 2011). These changes can

Responsible Editor: Eric Deleersnijder

E. Charles (✉) · D. Idier · G. Le Cozannet
BRGM, 3 Avenue Guillemin, 45060 Orléans Cedex 2,
France
e-mail: elodie.charles29@gmail.com

P. Delecluse
CNRM, Météo France, 73 Avenue de Paris,
94165 Saint-Mandé Cedex, France

M. Déqué
CNRM/GAME, Météo-France, 42 Avenue Coriolis,
31057 Toulouse, France

then impact the resulting wave climate, in terms of wave height, period and direction. Concerning wave climate, the Fourth Assessment Report (Christensen et al. 2007) yet highlighted a lack of information on the potential changes in regional wave climate. The few available global projections of wave climate show consistent results in the North Atlantic Ocean, with an increase of wave height in the southwestern part and in the northeastern part and a decrease in the central part (Wang and Swail 2006; Caires et al. 2006; Mori et al. 2010). However, the spatial extent, the significance and the amplitude of those changes largely depend on the season and greenhouse gases (GHG) emission scenario and on the model itself.

Focusing on the Bay of Biscay, the spatial resolution of these projections at global (Wang and Swail 2006; Caires et al. 2006; Mori et al. 2010) and at Atlantic Ocean basin scale (The WASA Group 1998; Wang et al. 2004; Leake et al. 2007) is insufficient (finest is 0.625° by 0.833°) to extract values inside the 4° by 4° area of the Bay of Biscay and along the coast. Some regional projections focusing on areas close to the Bay of Biscay were carried out at a higher spatial resolution. Debernard and Røed (2008) focus on Northern Seas and provide some results within the Bay of Biscay at a spatial resolution of 0.5° . Zacharioudaki et al. (2011) focus on the west-European shelf seas and provide some results west of the Bay of Biscay (the eastern boundary of Zacharioudaki et al. (2011) simulation domains is 2.8° W) at a spatial resolution of 0.2° . These regional projections indicate either no significant change or a decrease of wave heights in the Bay of Biscay, depending on the season. However, either the spatial coverage or the spatial resolution of these regional projections are still insufficient to assess the changes along the coast. Moreover, none of the referred studies investigates the changes of wave climate in terms of wave period and wave direction, variables which are required to study the impact of waves on the coastal area.

Thus, the aim of this study is to assess the global warming impact on wave climate within the Bay of Biscay, by investigating wave height, period, direction and wave type changes. Moreover, this study addresses the issue of the relation between those wave changes and wind changes.

The paper is organised as follows: Section 2 describes the method and datasets. Main results are presented in Section 3 both focused on regional and local changes. The wave climate changes are interpreted regarding the wind climate changes in Section 4. Section 5 extends the analysis of wave climate evolution towards the coast. Discussion and conclusion are presented, respectively, in Sections 6 and 7.

2 Method and datasets

Dynamical downscaling technique can provide wave fields at a high spatial resolution. Used successfully over other areas to investigate the impact of climate change on waves (e.g. Leake et al. 2007; Grabemann and Weisse 2008; Hemer et al. 2012), we apply this technique for the Bay of Biscay. Waves are simulated for three GHG emission scenarios—SRES A2, A1B and B1—on the period 2061–2100 and for a control scenario REF, corresponding to the observed GHG emissions on the period 1961–2000.

The Fig. 1 illustrates the main steps of the wave field production. Wind fields used to force a wave model and to produce the present and future wave fields are issued from the ARPEGE-Climat atmospheric GCM (Gibelin and Déqué 2003). The simulated wave fields are then corrected to remediate systematic biases induced by GCMs. This correction is constructed using the wave dataset BoBWA-10kH, representative of the present wave climate, which has been validated against in situ measurements of wave parameters (Charles et al. 2012). This dataset was modelled using the same dynamical downscaling system, forced by the ERA-40

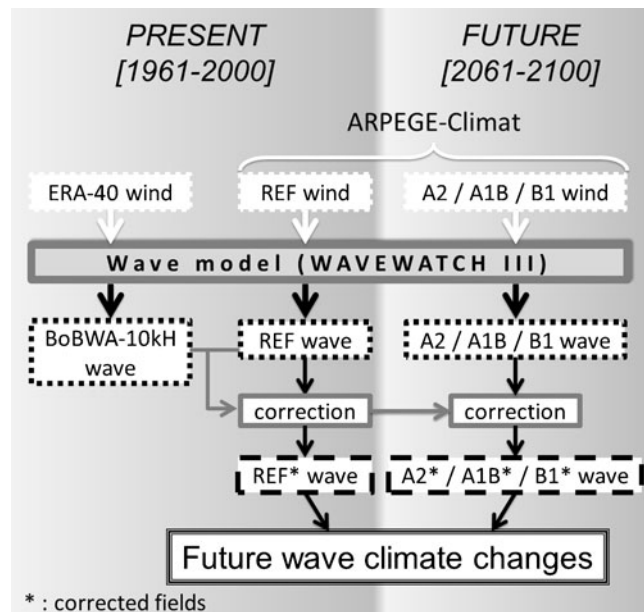


Fig. 1 Illustration of the main steps and datasets of the wave field production. Wave model is forced by 10-m wind fields of the ERA-40 reanalysis and of the simulations of ARPEGE-Climat (present control scenario REF and three future scenarios A2, A1B and B1) to simulate five wave datasets. A correction is built, based on BoBWA-10kH and REF wave fields during the period 1961–2000. This correction is then applied to REF, A2, A1B and B1 wave datasets to produce corrected wave datasets, called REF*, A2*, A1B* and B1*. Corrected wave datasets are used to investigate future wave climate change

reanalysis wind fields (Uppala et al. 2005). The correction is then applied to the four wave datasets generated by ARPEGE-Climat wind fields.

2.1 Wave dynamical downscaling

Projection of wave climate at regional scale is performed using the wave downscaling system developed in Charles et al. (2012). Waves are generated and propagated using the version 3.14 of the WAVEWATCH III wave model (WW3) (Tolman 2009) and the TEST441 source terms parameterization, described in Ardhuin et al. (2010). The wave model is implemented on two nested domains: the North Atlantic Ocean (spatial resolution of 0.5°) and the Bay of Biscay (spatial resolution of 0.1°) (Fig. 2).

Calibration and validation of the wave downscaling system forced by the ERA-40 reanalysis wind fields (Uppala et al. 2005) are described in Charles et al. (2012). The ERA-40 wind speed is underestimated and calibration consisted in increasing the wind speed to improve the modelled wave fields. Compared to eight buoy measurements along the Atlantic coast, the simulated wave fields are well reproduced in the Bay of Biscay area. Wave heights are particularly close to measurements, with a squared correlation coefficient ranging from 0.76 to 0.94, a root mean square error smaller than 39 cm and a bias ranging from -10 to 10 cm. However, the comparison also highlighted weakness to reproduce the wind sea directions and a systematic positive bias in mean wave period (from -0.17 to 1.27 s).

2.2 Forcing data

To simulate future wave conditions, the wave model is forced by the wind fields issued from the simulations of ARPEGE-Climat v4.6 atmospheric GCM (Gibelin and Déqué 2003). It provides wind fields for four different scenarios. The first one, REF, corresponds to observed radiative forcing (GHG emissions, aerosols) for the period 1950–2000. The three others are forced by the SRES A2 (high emission), A1B (mid-range emission) and B1 (low emission) scenarios for the period 2001–2100. Wind fields are available on a variable horizontal grid, with higher resolution over France (spatial resolution over the North Atlantic Ocean ranges from 60 to 80 km), every 6 h. For this study, wind fields are extracted for the present period 1961–2000 (REF) and future period 2061–2100 (A2, A1B and B1) and are interpolated on the two domain grids of the wave model.

2.3 Correction of simulated wave fields

GCMs exhibit systematic errors, inducing biases that propagate on wave fields. The direct comparison of past and future wave fields, modelled by the same model chain and hypothesis, gives information on changes amplitude. However, we cannot rely on the mean absolute values, and the amplitude of certain types of waves can be under- or over-estimated. It is thus relevant to correct this bias before using wave field in impact models. Existing studies of regional wave projections analyse directly the simulated waves (e.g. Leake et al. 2007; Grabemann and Weisse 2008; Lionello et al. 2008) or

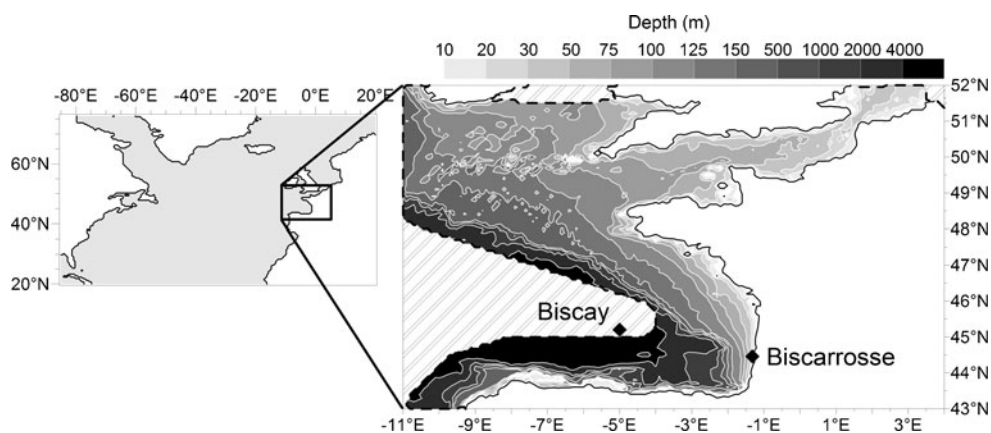


Fig. 2 Model domains used for the simulations with WW3 wave model: *left* North Atlantic Ocean domain (spatial resolution 0.5°) and *right* Bay of Biscay regional domain (spatial resolution 0.1°). *Hatched areas* (water depths larger than 4,000 m) are

excluded from the second domain. The *diamonds* indicate the position of the Biscay and the Biscarrosse buoys. The Biscay buoy is located in the North Atlantic computational domain

apply a correction on the wind forcing issued from the GCM (Wang et al. 2010; Hemer et al. 2012), or on the simulated wave fields (Andrade et al. 2007). Correcting the wind or wave fields implies a strong hypothesis on the GCM: We assume that the statistical properties of the GCM systematic errors are stationary, which is not demonstrated in the context of climate change and is itself a topic of research.

It is chosen to carry out the bias corrections on the simulated wave fields. Correcting the wave conditions instead of wind fields prevents from modifying the atmospheric circulation patterns: The atmospheric physics is preserved. Different methods of bias correction exist, such as correcting the bias of the mean value (e.g. Wang et al. 2010), but this does not take into account the distribution of wave conditions. The quantile–quantile correction, applied for different hydrological impact studies (e.g. Déqué 2007; Reichle and Koster 2004; Wood et al. 2002), corrects the probability density function of the simulated variable, quantile by quantile, adjusted to observations distribution.

This quantile–quantile correction is carried out independently on the wave height, period and direction. Considering that the model errors can depend on the season and location, the correction is built for each season and for each grid point. The wave dataset BoBWA-10kH developed and validated in Charles et al. (2012) stands as observations. It was computed with the same

wave model, forced by the ERA-40 wind fields, and will be called hereafter OBS.

Firstly, the correction C is built from the N quantiles of the variable X of REF and OBS datasets:

$$C_q = X_q^{\text{OBS}} - X_q^{\text{REF}}, \quad q = 1, N \quad (1)$$

Significant wave height and mean wave period are corrected on the percentiles (0.01 to 0.99 quantiles). To better correct the sides of the distribution, the 0.005 and 0.995 quantiles are added, resulting in 101 quantiles. Concerning the mean wave direction, the time series of directions for a point and a season are first rotated to be centered on the predominant direction, and then the correction is performed on the per milles (0.001 to 0.999 quantiles) and on the 0.0005 and 0.9995 quantiles (1001 quantiles). When the same direction is obtained for consecutive quantiles, the correction is averaged for these quantiles. Mean wave directions issued from the grid are given with 1° precision and present high density around the predominant direction (as illustrated in Fig. 3c, at the Biscay buoy, 70 % of the winter waves are coming from the west northwest octant). Increasing the quantiles number allows to better define the intervals in which the direction increments and then to prevent from getting gaps in the corrected distribution.

Secondly, the correction is applied to the time series of the variable X issued from the REF, A2, A1B and B1 datasets:

$$\begin{aligned} X^*(t) &= X(t) - C_1 \quad \forall X(t) < X_1^{\text{REF}} \\ X^*(t) &= X(t) - C_q \quad \forall X(t) \in [X_{q-1}^{\text{REF}}; X_q^{\text{REF}}[, \quad q = 2, N-1 \\ X^*(t) &= X(t) - C_N \quad \forall X(t) \geq X_N^{\text{REF}} \end{aligned} \quad (2)$$

This quantile–quantile technique modifies the probability density function of the REF wave conditions so that it superimposes on the OBS probability density function. For instance, Fig. 3 compares the histograms

of each corrected variable at the Biscay buoy during winter. Without correction, the occurrence of wave heights larger than 6 m is underestimated as well as the occurrence of mean wave periods larger than 12 s,

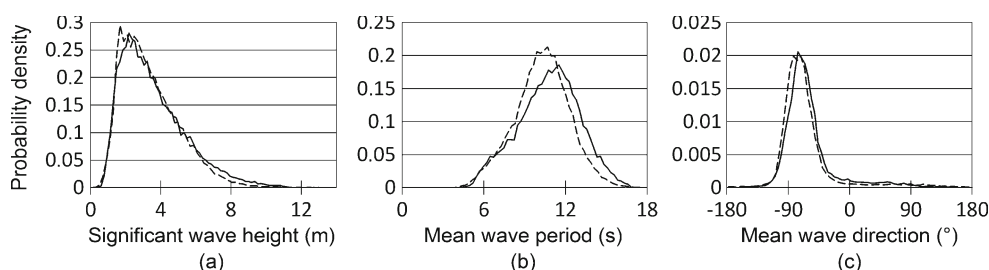


Fig. 3 Probability density functions of **a** significant wave height, **b** mean wave period and **c** mean wave direction at the Biscay buoy during winter 1961–2000 for the OBS dataset (plain line)

and the raw REF dataset (dotted line). Once corrected, the REF cumulative distribution functions superimpose on the OBS ones

and the mean wave directions ranging from -100° to 0° are slightly anti-clockwise shifted. Those differences between REF and OBS wave field distributions are corrected by this quantile–quantile technique.

3 Results

In this section, we analyse corrected wave fields, and the REF, A2, A1B and B1 wave datasets will refer to the corrected wave fields. Three potential future scenarios of wave climate are investigated, with a more thorough analysis for the higher emission A2 scenario. Using the higher emission scenario is useful to amplify the differences with present climate and may not be the most unrealistic.

To quantify the future changes, differences between the present (1961–2000) and the future (2061–2100) corrected wave conditions are computed for each meteorological season—winter (December, January, February), spring (March, April, May), summer (June, July, August) and autumn (September, October, November). Wave climate changes are firstly assessed at regional scale, in the Bay of Biscay, and secondly at local scale, at the location of the offshore Biscay buoy, in the central part of the Bay of Biscay at 4,500 m depth (Fig. 2).

3.1 Regional changes

Figure 4 shows the seasonal mean wave conditions for the present REF scenario (1961–2000) and its differences with the future A2 scenario (2061–2100). Wave direction is the direction from which waves come measured clockwise from north.

A general significant decrease of wave heights is noticeable for all seasons within the Bay of Biscay. Modest changes occur during winter. Indeed, in the Bay of Biscay, wave heights (with a seasonal mean ranging from 2 to 3.5 m) present a significant decrease ranging from -5 to -15 cm while mean wave periods and directions remain rather stable. During autumn and spring, wave heights (seasonal mean ranging from 1.5 to 2.5 m) exhibit a significant decrease ranging from -10 to -20 cm, mean wave periods slightly decrease during spring (up to -0.3 s) while mean wave directions are stable. Main changes occur during summer: wave heights, with a seasonal mean ranging from 1 to 1.5 m, present a significant decrease ranging from -10 to -20 cm. During summer, mean wave periods slightly decrease (-0.5 s) and mean wave directions present a strong northerly shift ranging from 3 to 10° . This is beyond the model resolution, which is 15° . However, these changes should be noteworthy. The direction dataset is not precise, but because we use long time series, it appears to be accurate enough to capture

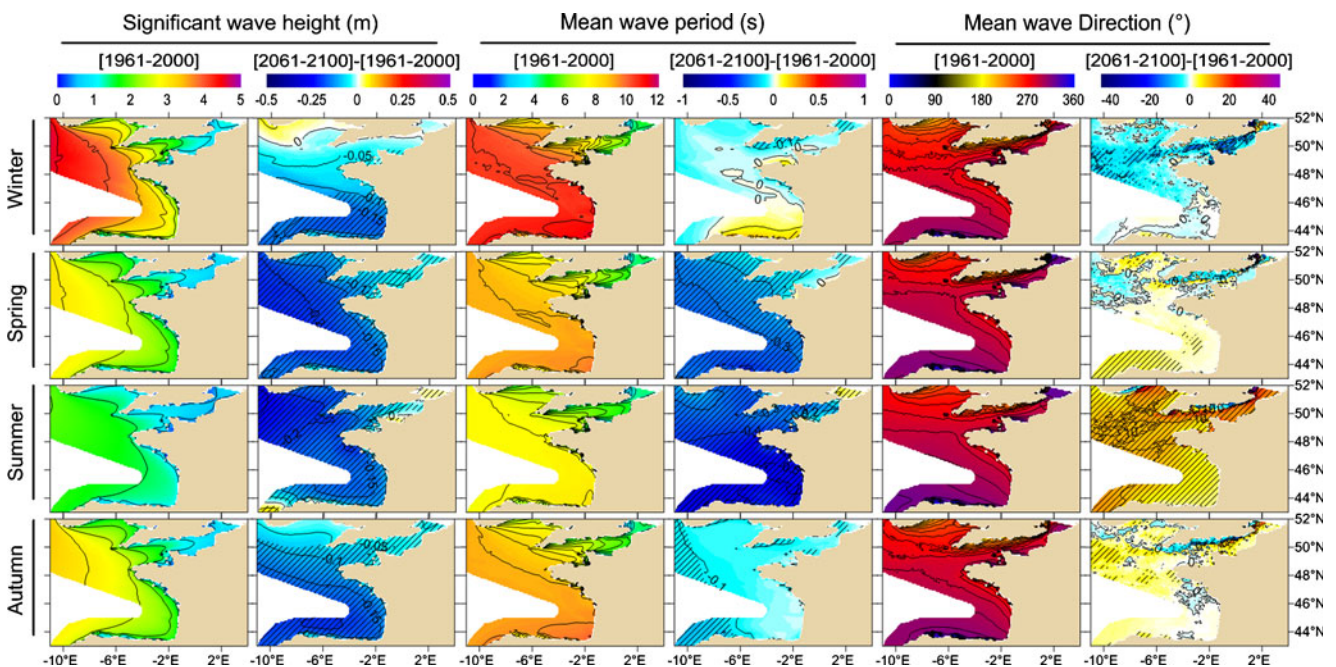


Fig. 4 Maps of corrected seasonal significant wave height, mean wave period and mean wave direction for the present scenario REF (respectively, *first, third and fifth columns*) and differences between the future scenario A2 (2061–2100) and the present

scenario REF (1961–2000) (respectively, *second, fourth and sixth columns*). Hatching indicates changes significant at more than 95 %

slight changes in directions (that will be related to wind changes in Section 4).

Changes for the lower emission scenarios A1B and B1, as well as changes for extreme waves (higher than the 95th percentile) are detailed in Table 1. Displayed values correspond to the spatial average of wave conditions inside the Bay of Biscay, eastward 4° W. The extreme waves (higher than the 95th percentile) tend to exhibit the same sign and amplitude of changes as the mean waves. However, the summer 95th percentile of wave heights exhibits a strong decrease of about −20.6 % for the A2 scenario that is twice the mean wave height decrease. The major changes found for the A2 scenario are generally also found for the two other scenarios, but with a smaller amplitude for the A1B scenario and even smaller amplitude for the B1 scenario. This result shows that the differences between present and future wave climate are larger when the GHG emissions increase. During winter, B1 scenario projected changes (wave height increase) differ from the two other scenarios. This projected increase in the Bay of Biscay can be explained by smaller changes of atmospheric conditions within the North Atlantic Basin. The above results are obtained analysing the corrected waves. It is worthwhile to notice that changes were also calculated for uncorrected waves (not shown here) and gave very similar results, with a larger clockwise shift of summer wave directions (+7° for A2 mean summer waves, to be compared with the 5.1° of Table 1).

3.2 Local changes

To better assess which type of wave is impacted and how it is impacted by climate change, we focus on

the offshore Biscay buoy, located at 5° W, 45.201° N at 4,500 m depth (Fig. 2). Bivariate diagrams of wave densities (distribution of wave heights against periods and of wave heights against directions) are investigated for each season. To calculate wave densities, bivariate diagrams are divided into cells of 1 m, 1.25 s and 18°, respectively, for significant wave heights, mean periods and mean directions. The changes between the future scenario A2 and present climate scenario REF are assessed by subtracting the present climate bivariate diagram of density from the future one. Only significant changes are considered (changes significant at more than 95 % according to Student's *T* test, when comparing the cell mean occurrence changes with the interannual variations of the cell future occurrence).

To better determine the wave characteristics changes, steepness and energy flux are calculated, using the same formulations as those used by Charles et al. (2012). The median values of the REF annual dataset energy flux and steepness are calculated (respectively, 19 kW m^{−1} and 1/58 at the Biscay buoy) and plotted on bivariate diagrams, as well as the Pierson–Moskovitz steepness ($\epsilon = 1/19.7$ is the theoretical steepness of fully developed wind sea). The median energy flux splits the wave dataset into a half of most energetic waves on the right and a half of less energetic waves on the left (Fig. 5). Steepness is used in this section to distinguish swell from wind sea. Swell usually presents a smaller steepness than wind sea. At the Biscay buoy, we assume that approximately 50 % of the waves presenting the smallest steepness are swell (Butel et al. 2002; Le Cozannet et al. 2010). Waves above the median steepness on Fig. 5 are then considered as swell. These swell propagated across the

Table 1 Wave condition changes averaged on an area in the Bay of Biscay (eastward 4° W)

For each season, the first line indicates the mean wave conditions (mean and 95th percentile of wave height) for the present scenario REF (1961–2000). The three following lines give the difference between the wave conditions (mean and 95th percentile of wave height) of the present REF (1961–2000) and of each future scenario (2061–2100) relative to the present scenario

			Significant height		Mean period		Mean direction	
			Mean	H95th	Mean	H95th	Mean (deg)	H95th (deg)
Winter	REF		2.8 m	6.5 m	10.8 s	12.4 s	287	280
	B1		1.3 %	2.8 %	2.6 %	2.4 %	−0.9	−0.3
	A1B		−4.4 %	−3.5 %	1.2 %	1.8 %	0.3	0.1
	A2		−4.7 %	−0.9 %	0.4 %	2.1 %	−0.5	−0.7
Spring	REF		1.9 m	4.9 m	9.2 s	11.2 s	293	280
	B1		−1.1 %	−2.3 %	−1.0 %	1.5 %	−0.2	0.5
	A1B		−4.3 %	−5.7 %	−1.7 %	−0.6 %	0.6	1.5
	A2		−7.6 %	−7.1 %	−3.3 %	−1.2 %	1.2	0.4
Summer	REF		1.3 m	2.8 m	7.7 s	8.9 s	296	285
	B1		−4.3 %	−8.1 %	−2.9 %	0.2 %	3.7	2.9
	A1B		−9.7 %	−20.1 %	−6.8 %	−3.1 %	6.1	7.5
	A2		−11.4 %	−20.6 %	−6.4 %	−5.1 %	5.1	7.4
Autumn	REF		2.0 m	5.0 m	9.3 s	11.4 s	292	281
	B1		−3.6 %	−1.2 %	−1.0 %	0.0 %	1.7	0
	A1B		−8.5 %	−6.0 %	−0.7 %	−0.9 %	1.8	0.5
	A2		−7.7 %	−8.7 %	−0.3 %	0.3 %	0.3	0.7

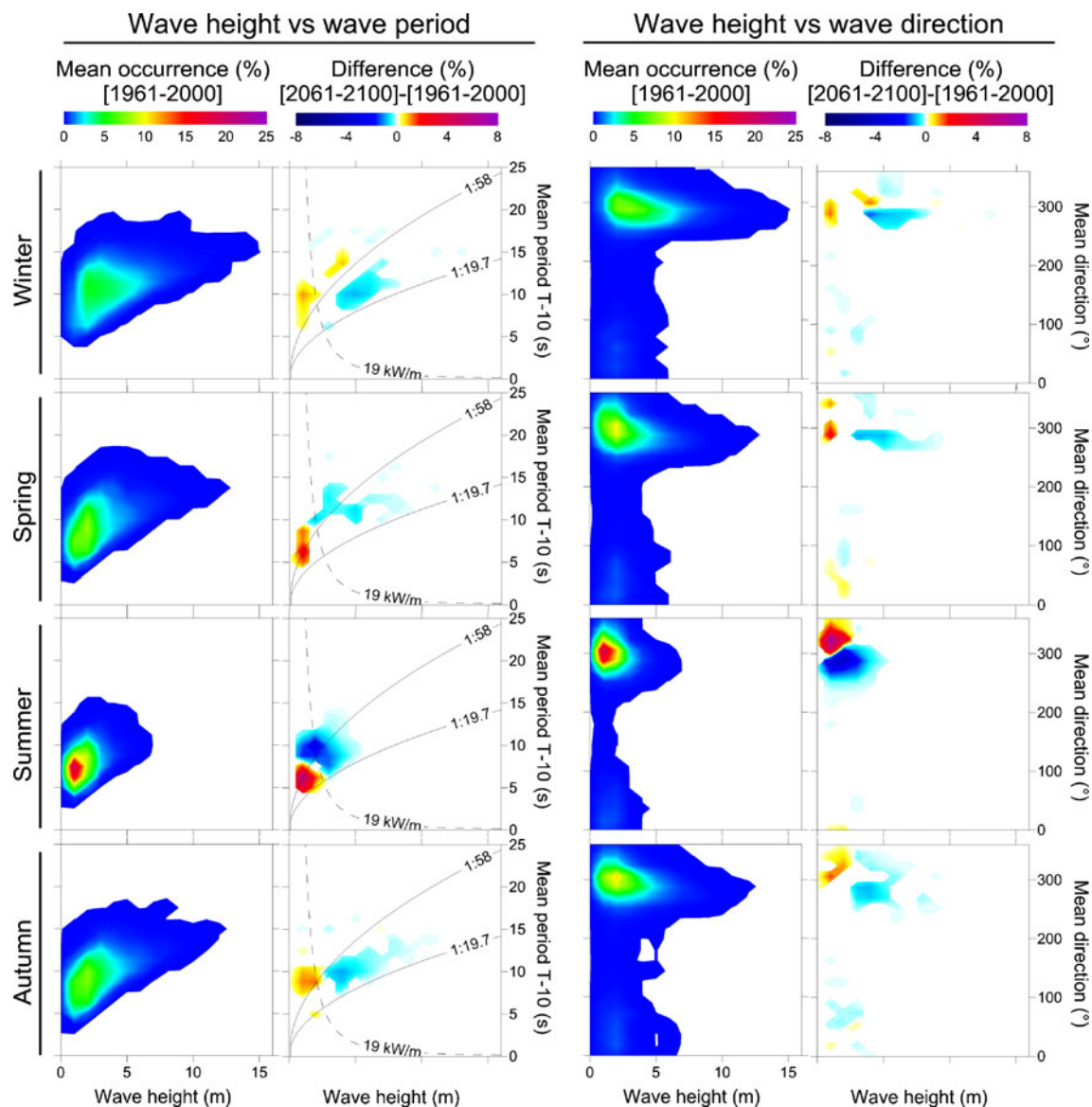


Fig. 5 Bivariate diagrams of corrected wave conditions at the offshore Biscay buoy (4,500 m depth) for the present REF scenario (1961–2000) and bivariate diagrams of changes between wave conditions of the future A2 scenario (2061–2100) and the present REF scenario (1961–2000). Only changes significant at

more than 95 % (Student's *T* test) are plotted. *Plain lines* indicate the median and the Pierson–Moskovitz steepness, and *dotted line* indicates the median energy flux, calculated from the REF dataset

eastern part of the Atlantic basin, accounting for their attenuated patterns (small height for large period). Wind sea steepness is close to the Pierson–Moskovitz steepness (waves are around the 1/19.7 steepness on Fig. 5). Intermediate waves are generated in areas closer than swell and further than wind sea generation areas and then present an intermediate steepness (waves are between median and Pierson–Moskovitz steepnesses in Fig. 5).

The bivariate diagrams shown in Fig. 5 illustrate the REF scenario (1961–2000) and its difference with the future A2 scenario (2061–2100) at the Biscay buoy.

Concerning the changes between present and future climate, the wave density patterns are particularly impacted during summer. A decrease of energetic waves (large wave height and period) occurs while non-energetic waves are increasing. Concerning wave directions, the small waves coming from the north-northwest (from 300° to 360°) occur more frequently as larger waves coming from the west (from 250° to 310°) occur less frequently during the A2 scenario than during the present climate. These changes lead to a decrease of wave energy and a northerly shift of wave direction during summer.

During winter, the occurrence of swell increases while the occurrence of intermediate waves decreases. One can notice that large waves (higher than 2.5 m) coming from 260° to 300° are more frequent while those coming from 300° to 330° are less frequent. Waves larger than 2.5 m present a slight northerly shift, which was not noticeable at regional scale.

During spring and autumn, the changes are less pronounced than during summer, but the pattern is the same. The occurrence of small non-energetic waves increases while the occurrence of large energetic waves decreases.

4 Analysis of wave climate changes regarding wind field changes

The above wave changes in the Bay of Biscay are related to wind changes in the North Atlantic Ocean and in the Bay of Biscay. This section aims to better understand which wind changes lead to which wave changes. We focus on winter and summer changes between REF and A2 scenarios, as wave changes are quite different and highlight different mechanisms. Thus, the interpretation of changes is done first during winter and second during summer. Moreover, we must notice that the correction performed on simulated waves implies that they are not directly linked to the wind fields used to force the wave model. Therefore, we investigate here the relation between uncorrected waves and wind.

4.1 Method: relating waves to wind generation areas

Wave bivariate diagrams highlight different changes depending on the wave type (swell, intermediate waves and wind sea). Moreover, each type of wave can be related to different wind generation areas, more or less distant from the point of observation.

Therefore, the first step of this analysis is to extract each type of wave from the wave time series. For each season, the analysed type of waves (swell, wind sea or intermediate waves) is extracted from the uncorrected wave time series at the Biscay buoy. There are different methods to distinguish swell from wind sea, such as wave steepness, used in Section 3, or wave age, used in several wave climate studies (Hanley et al. 2010; Semedo et al. 2011). In this section, we compare uncorrected waves to uncorrected wind, so it is consistent to use wave age criterion, which considers local wind speed and direction. The wave age criterion allows to

determine if the local wind is generating and increasing local waves or not. More precisely, we use a selection criterion based on the inverse wave age, with associated wave types defined as:

$$A^{-1} = \frac{U_{10} \cos(\theta_{\text{wave}} - \theta_{\text{wind}})}{C_p} \quad \text{with } C_p = \frac{gT_p}{2\pi} \quad (3)$$

$$\text{Swell: } A^{-1} < 0.15$$

$$\text{Intermediate waves: } 0.83 < A^{-1} < 0.15$$

$$\text{Wind sea: } A^{-1} > 0.83$$

Inverse wave age depends on the local wind speed U_{10} and direction θ_{wind} and is an index of the wind speed compared to the wave peak phase speed C_p .

According to the swell wave age criterion, swell corresponds to counterswells ($A^{-1} < 0$, difference between swell and wind directions larger than 90°) and waves propagating at a phase speed C_p higher than 6.7 times the wind speed. Wind sea wave age criterion selects waves propagating with a maximum angle of 90° around the wind direction and at a phase speed smaller than 1.2 times the wind speed. The intermediate waves are selected as the remaining waves which neither are swell nor wind sea.

Wind sea is generated by local wind. Intermediate waves and swell are generated, respectively, within the Bay of Biscay and its neighbourhood and in the North Atlantic Ocean. To characterize more precisely in which areas of the Bay of Biscay and North Atlantic, intermediate waves and swell are generated, we use the wave direction information. We assume that swell and, to a certain extent, intermediate waves propagate straightforward along the shortest path between the generation area and the point of observation (e.g. Gjevik et al. 1988). The shortest path between two points on the globe follows a great circle (circle intersecting the Earth center). Each wave direction at the Biscay buoy is then associated to a single path. Figure 7 shows great circles presenting different angles when intersecting the Biscay buoy (red lines). Great circle label indicates the direction of swell that propagated along the circle when arriving at the Biscay buoy (the direction is not constant along a great circle).

Therefore, the second step of this analysis is to classify waves at the Biscay buoy into 16 direction bins. Those direction bins are called hereafter by the initials of the cardinal and ordinal directions (for instance NNE for north-northeast, corresponding to 22.5° direction).

4.2 Winter wave changes and their relation with wind changes

During winter, as shown in Section 3.2, main identified wave changes concern intermediate waves and swell (Fig. 5). Therefore, winter intermediate waves and swell are extracted and classified (Fig. 6) following the above method, and their relation with regional and basin-scale wind changes (Fig. 7) is investigated.

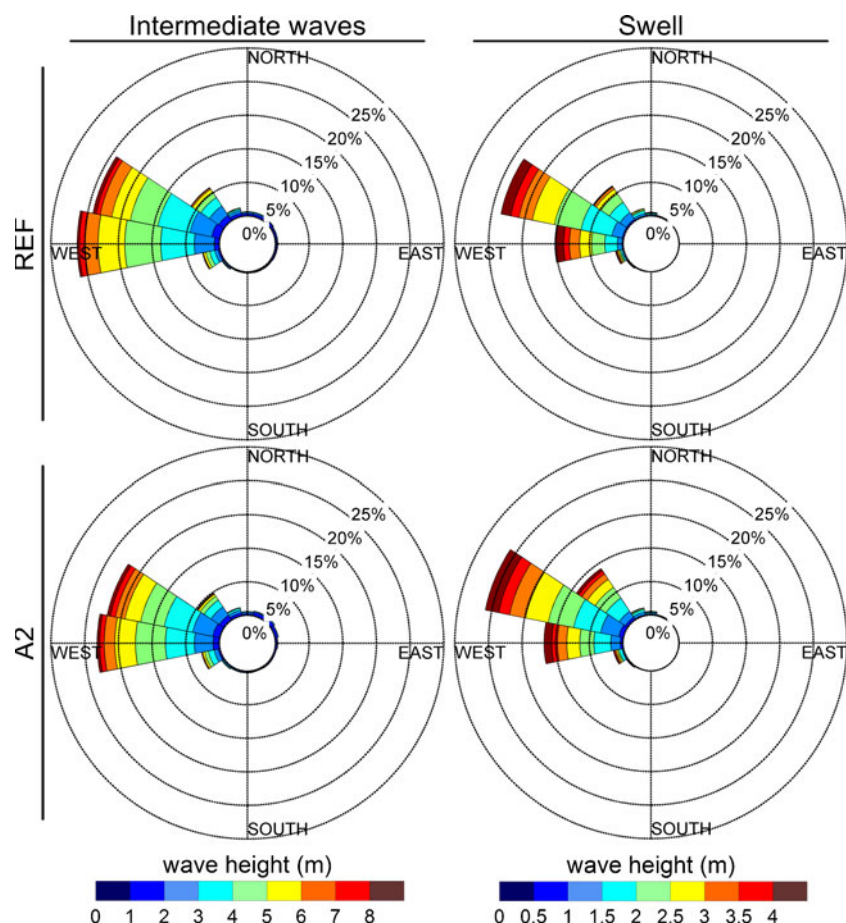
Nearly half of the winter waves are intermediate waves (54 % for the REF scenario and 49 % for A2 scenario). More than 70 % of those intermediate waves are coming from the W and WNW direction bins. Comparison of REF and A2 wave roses highlights no significant changes in wave height or direction distribution, except a general decrease of occurrence. This decrease was also underlined for corrected waves in Fig. 5.

Winter wind within the Bay of Biscay and its neighbourhood is blowing from the southwest direction (Fig. 7). The large fetch in the western part of the Bay of Biscay and the predominant wind direction induce that

intermediate waves are mainly propagating from the west in the Bay of Biscay. Comparison of REF and A2 scenario regional wind (Fig. 7) shows a significant decrease of wind speed in the Bay of Biscay, south of 46° (-0.7 m s^{-1} at the Biscay buoy and up to -0.9 m s^{-1}). Therefore, the projected decrease of the intermediate wave occurrence at the Biscay buoy (from 54 % for REF scenario to 49 % for A2 scenario) could be related to winter regional wind that would be less efficient at generating waves in future A2 scenario.

Concerning swell, about 40 % of waves at the Biscay buoy are classified as swell. Ninety percent of swell is shared between the W, WNW and NW direction bins, with 48 % coming from the WNW direction (Fig. 6). Comparison of REF and A2 distributions first highlights a general increase of swell occurrence (respectively, 39 % and 46 % of REF and A2 uncorrected winter waves). Although swell occurrence increases in each direction bin, one can notice that there are changes in the distribution of wave height. The occurrence of small swell (wave height smaller than 2 m)

Fig. 6 Directional distribution of winter intermediate waves (*left*) and swell (*right*) at the Biscay buoy for the present REF climate (1961–2000) and future A2 scenario (2061–2100). Colours indicate wave height distribution in each direction bin. Percentages are given for the whole winter dataset



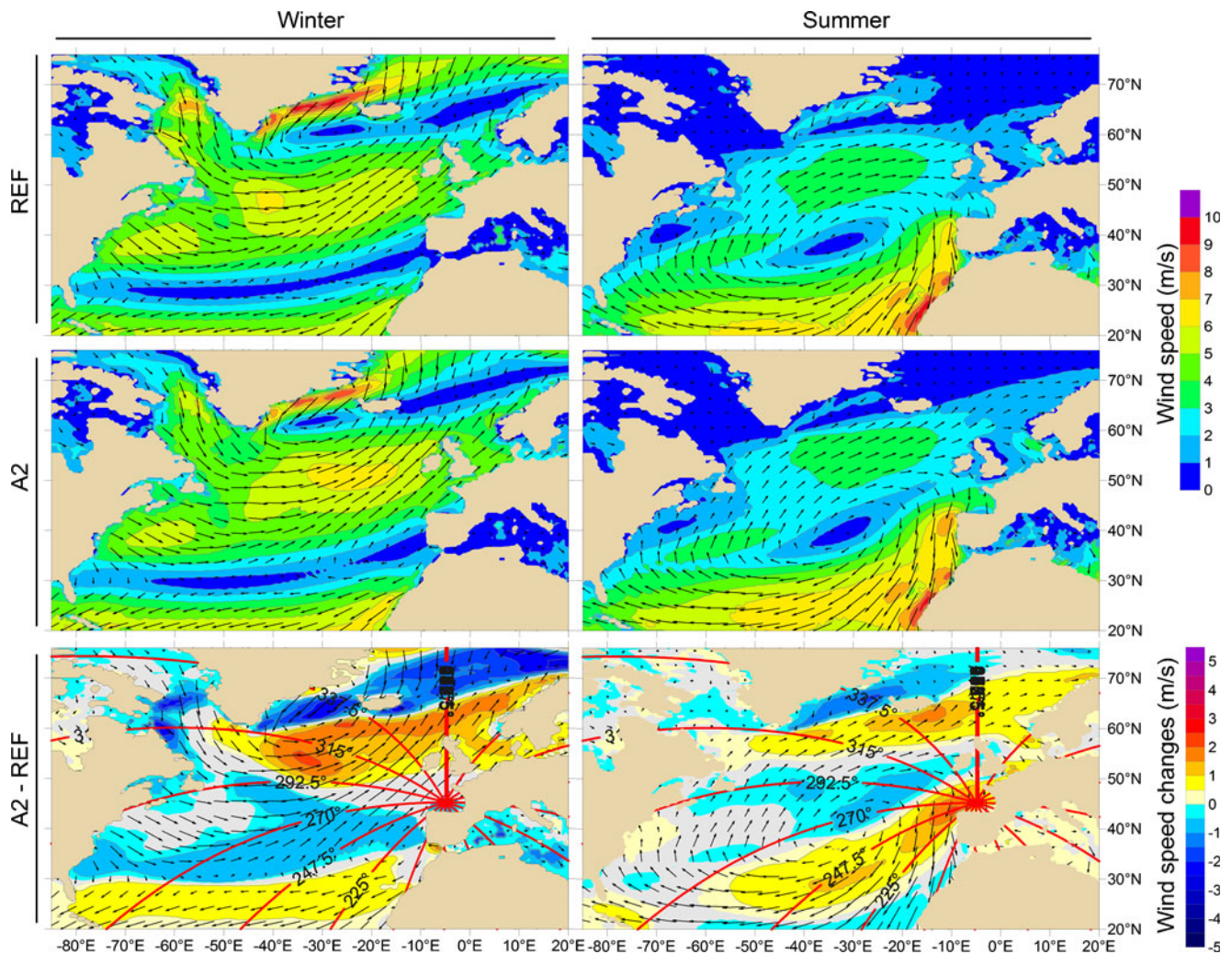


Fig. 7 Winter (left) and summer (right) mean wind fields over the North Atlantic Ocean for the present climate (1961–2000) and the future A2 scenario (2061–2100), issued from ARPEGE-Climat simulations. Last row is the difference between present and future (grey areas indicate wind speed changes not significant

at 95 %). Arrows give the wind mean direction and are scaled with wind speed (last row arrows are future A2 scenario wind conditions). Great circles intersecting the Biscay buoy are indicated by red lines and the corresponding wave direction at the Biscay buoy by black labels

coming from the W direction increases and the occurrence of large swell (wave height larger than 2.5 m) coming from the NW direction increases (Fig. 6). These results were also highlighted by the bivariate diagram of corrected waves at the Biscay buoy (Fig. 5).

Figure 7 shows winter mean wind fields and changes over the North Atlantic Ocean for the REF and A2 scenarios. First, one can notice that stronger winds are located in the central part of the North Atlantic Ocean, between 40° N and 60° N. This is consistent with the swell W, WNW and NW predominant direction bins. Corresponding swell trajectories (270°, 292.5° and 315° great circles) indeed cross strong wind areas, without encountering land. Concerning projected wind changes,

the strong wind core in the central North Atlantic shifts northeastward and intensifies for the A2 scenario (Fig. 7). This shift results in a significant increase of wind speeds north of 50° N and a significant decrease between 30° N and 50° N.

The increase of large swell occurrence coming from the NW direction bin would then be due to the increase of wind speed along the 315° great circle. The increase of small swell occurrence coming from the W direction would be induced by two processes: the decrease of wind speed along the corresponding great circles and the decrease of local wind speed in the Bay of Biscay. Moreover, the general increase of swell occurrence can be partly related to the local wind speed decrease in

the Bay of Biscay: Wind is less efficient at generating waves locally, and non-energetic swell systems become predominant in the wave spectrum.

In conclusion, the projected clockwise shift of large swell directions in the Bay of Biscay can be related to the northeastward shift of strong winds in the North Atlantic Ocean. The decrease of intermediate wave and increase of swell occurrences can be related to the decrease of wind speed in the Bay of Biscay towards the end of the twenty-first century.

4.3 Summer wave changes and their relation with wind changes

During summer, wind sea, intermediate waves and swell exhibit significant changes between REF and A2 scenarios at the Biscay buoy (Fig. 5). Therefore, the three types of wave are investigated regarding their relation with local-, regional- and basin-scale wind changes. Firstly, we investigate more thoroughly the wind sea changes at the Biscay buoy and associated local wind changes (Figs. 8 and 9). Secondly, we investigate intermediate wave changes in the Bay of Biscay and associated regional wind changes (Figs. 8 and 10). We finally give some elements to better understand

the link between swell and wind changes in the North Atlantic.

Summer wind sea occurrence remains constant between REF and A2 scenarios (respectively, 5.4 and 5.2 %). Comparison of present REF and future A2 wave roses highlights that occurrence and wave height of wind sea coming from the W direction bin are decreasing while they are increasing for wind sea coming from the N and NNE direction bins (Fig. 8). In Section 3, using corrected bivariate diagrams (Fig. 5), we also found that small waves coming from the North were more frequent and large waves coming from the west were less frequent in the future A2 scenario. However, no significant changes were exhibited for waves coming from the northeastern and southeastern quarters.

To relate wind sea changes to wind changes, wind speed and direction distributions at the Biscay buoy are shown on wind roses with 16 direction bins (Fig. 9) for present REF and future A2 scenarios. During present climate, local wind comes from two main sectors: west and northeast. Wind coming from W, WNW and WSW direction bins (about 23 % of occurrence) exhibits the largest wind speeds while wind coming from NE, NNE and ENE direction bins exhibits the largest occurrence (about 40 % of occurrence).

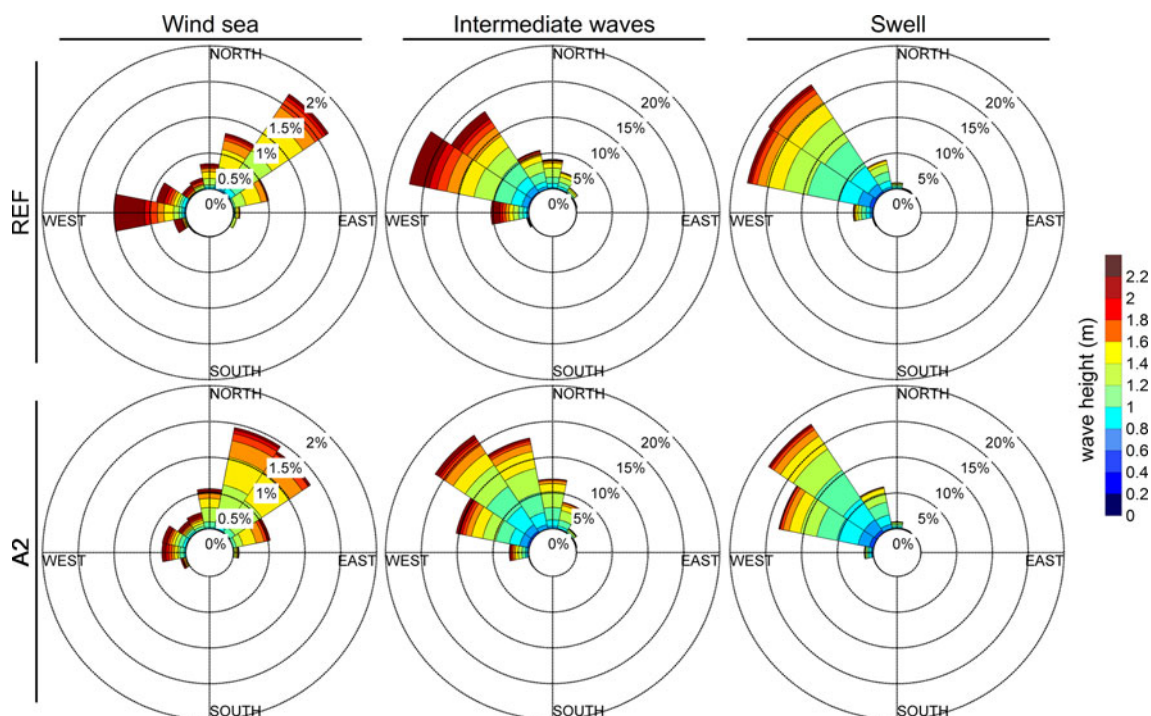


Fig. 8 Directional distribution of summer wind sea (left), intermediate waves (middle) and swell (right) at the Biscay buoy for the present REF climate (1961–2000) and future A2 scenario

(2061–2100). Colours indicate wave height distribution in each direction bin. Percentages are given for the whole summer dataset

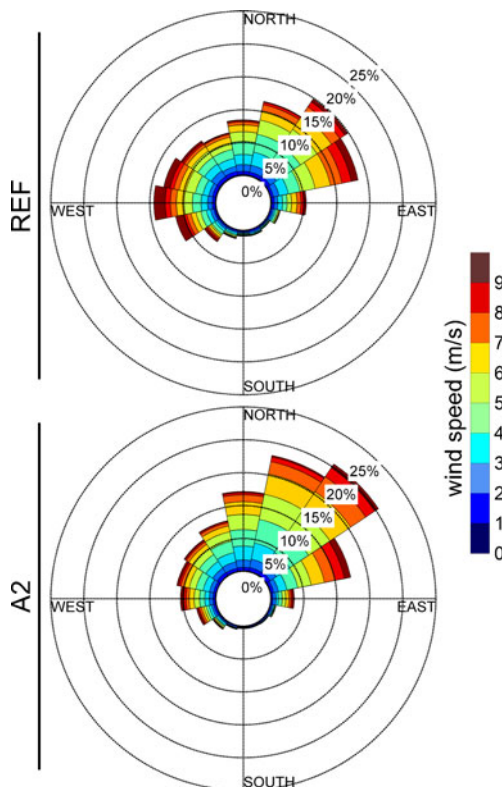


Fig. 9 Directional distribution of summer wind at the Biscay buoy for the present REF climate (1961–2000) and future A2 scenario (2061–2100). Colours indicate wind speed distribution in each direction bin

For future A2 climate, wind coming from West considerably decreases in terms of occurrence (W, WNW and WSW wind occurrence is about 14 %) and intensity, while NE wind occurrence increases (NE, NNE and ENE wind reach 51 %). Extreme winds are less frequent in future A2 climate (4 % of wind speeds higher than 9 m s^{-1}) than during present REF climate (7 % of wind speeds higher than 9 m s^{-1}). Wind is more efficient at generating waves as the wind direction is more stabilized in A2 than in REF scenario (the resulting vector presents a larger magnitude). However, the wind energy slightly decreases (summer root mean square wind speed at the Biscay buoy equals 5.7 m s^{-1} during REF scenario and 5.5 m s^{-1} during A2 scenario).

The decrease of wind sea height and occurrence in the W direction bin (Fig. 8) can thus be explained by the wind occurrence decrease in the W direction bin (Fig. 9) as well as the wind sea height and occurrence increase in the N and NNE direction bins can be related to the wind occurrence increase in the N and NNE direction bins. Moreover, the general decrease of wind sea heights and more particularly the decrease

of largest wave heights occurrence can be related to the decrease of extreme wind speed occurrence at the Biscay buoy and to the fetch reduction (wind blowing from NE direction in the Bay of Biscay will have a shorter fetch than wind blowing from W direction).

Regarding intermediate waves, their directional distribution (Fig. 8) indicates that they are largely coming from the NW quarter, with the largest waves coming from WNW direction bin. Intermediate wave roses exhibit an increase in wave occurrence between REF and A2 scenarios (respectively, 49 and 54 % of waves are intermediate waves). Comparing the present and future wave height and direction distributions, intermediate waves coming from the NNW, N and NNE direction bins are much more frequent, while waves coming from the W and WNW direction bins are less frequent and exhibit a significant wave height decrease. Intermediate waves coming from the NW direction bin are slightly more frequent, while their wave height decreases in the A2 scenario.

The investigation of related regional wind in the Bay of Biscay (Fig. 10) highlights an intensification of wind, with an increase of mean vector magnitude and a clockwise shift of vector direction.

The mean direction of winds that generate intermediate waves along the 270° and 292.5° great circles is clockwise shifted and present an angle larger than 90° with the great circle, which means that this wind is less successful in generating waves that can reach the Biscay buoy. This change of wind direction could explain the strong decrease of intermediate wave occurrence and wave height in the W and WNW direction bins. On the contrary, the clockwise shift of wind directions and the intensification of winds along the 0° , 337.5° and 22.5° great circles favor generation of waves that can reach the Biscay buoy. It may then explain the increase of intermediate wave occurrence in the N, NNW and NNE direction bins.

Summer swell (Fig. 8) exhibits two predominant directions, WNW and NW, which are clockwise shifted relative to winter swell directions. Summer swell wave height generally decreases, between REF and A2 scenarios. Concerning the direction distribution changes, one can notice that the occurrence of swell coming from the WNW and W direction bins decreases, while the occurrence of swell coming from the NNW direction bin slightly increases, resulting in a clockwise shift of swell direction. The occurrence of swell coming from the NW direction bin remains constant.

During summer, as well as during winter, the strong wind core in the central North Atlantic Ocean is shifted northeastward, resulting in an increase of wind

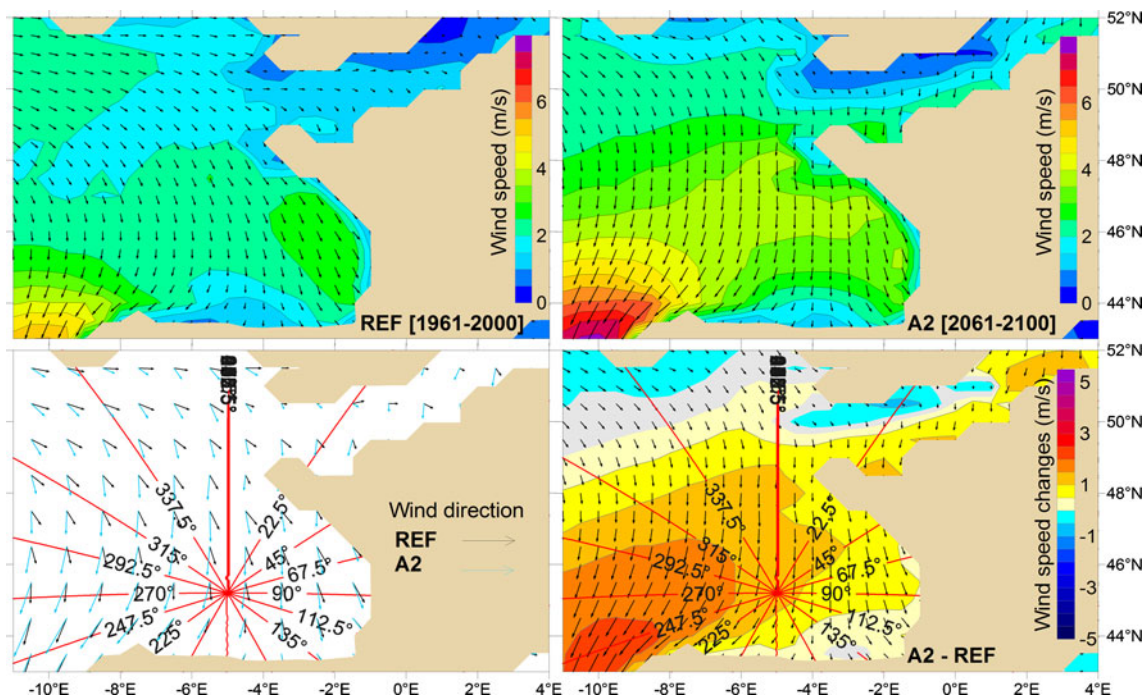


Fig. 10 Top summer mean wind fields in the Bay of Biscay during present climate (1961–2000) and future A2 scenario (2061–2100). Arrows give the wind mean direction and are scaled with the scenario wind speed. Bottom superposition of present and future summer wind directions (left) and difference between

present and future summer wind speed (arrows give future A2 wind conditions, grey areas indicate wind speed changes not significant at 95 %) (right). Great circles intersecting the Biscay buoy are indicated by red lines and the corresponding wave direction at the Biscay buoy by black labels

speeds north of 55° N and a decrease between 40° and 50° N. The decrease of the occurrence and wave height of WNW and W swell could then be related to the decrease of wind intensity along the 292.5° and the 270° great circles. Concerning the NW and NNW swell changes, it is more difficult to relate them to wind changes as swell crosses generation areas outside the Bay of Biscay presenting both a decrease and an increase in wind intensity.

To summarize, the general clockwise shift of wave directions during summer can be related to:

- The clockwise shift of local wind direction, leading to a clockwise shift of wind sea direction
- The clockwise shift of wind directions in the western part of the Bay of Biscay, which generates less intermediate waves propagating towards the French Atlantic Coast
- The clockwise shift of wind directions at the north of 48° N, which generates more intermediate waves propagating towards the Bay of Biscay and the Biscay buoy
- The decrease of wind intensity along the 270° and 292.5° great circles, leading to a decrease of W and WNW swell occurrence.

Regarding the general decrease of wave heights during summer, we can relate it to:

- The decrease of local extreme wind occurrence and particularly from the west, leading to a decrease in the highest wave occurrences
- The clockwise shift of wind directions in the western part of the Bay of Biscay disfavours the generation of higher waves by decreasing the fetch of the strong westerlies
- The decrease of wind intensity along the 270° and 292.5° great circles, leading to a decrease of W and WNW swell wave height.

The wave climate in the Bay of Biscay is then impacted by wind changes occurring at different spatial scales. Projected wave changes are directly related to determined wind changes.

5 Impact of climate change on coastal dynamics

In this section, we investigate how the offshore wave changes propagate towards the coast. We focus on the coastal Biscarrosse buoy, located at 1.32° W, 44.46° N

at 26 m depth (Fig. 2), 5 km offshore the Biscarrosse sandy beach.

Bivariate diagrams are shown on the Fig. 11. The median values of the REF annual dataset energy flux and steepness are calculated (respectively 8 kW m^{-1} and $1/99$ at the Biscarrosse buoy). As at the Biscay buoy, we assume that the waves presenting a steepness smaller than the median value are swell.

First, one can notice that the mean occurrence patterns between the offshore Biscay buoy (Fig. 5) and the coastal Biscarrosse buoy (Fig. 11) are not the same.

Waves approaching the coast are dissipated by the bottom friction (especially the high winter waves) and are refracted. Thus, the wave direction range is narrowed and wave heights are smaller at the Biscarrosse buoy than at the Biscay buoy. The wave period range remains constant when approaching the coast and is still comprised between 2 and 20 s.

Concerning the projected wave changes, bivariate diagrams of wave height versus wave period exhibit density changes very similar to the Biscay buoy identified changes. Winter swell is more frequent and winter

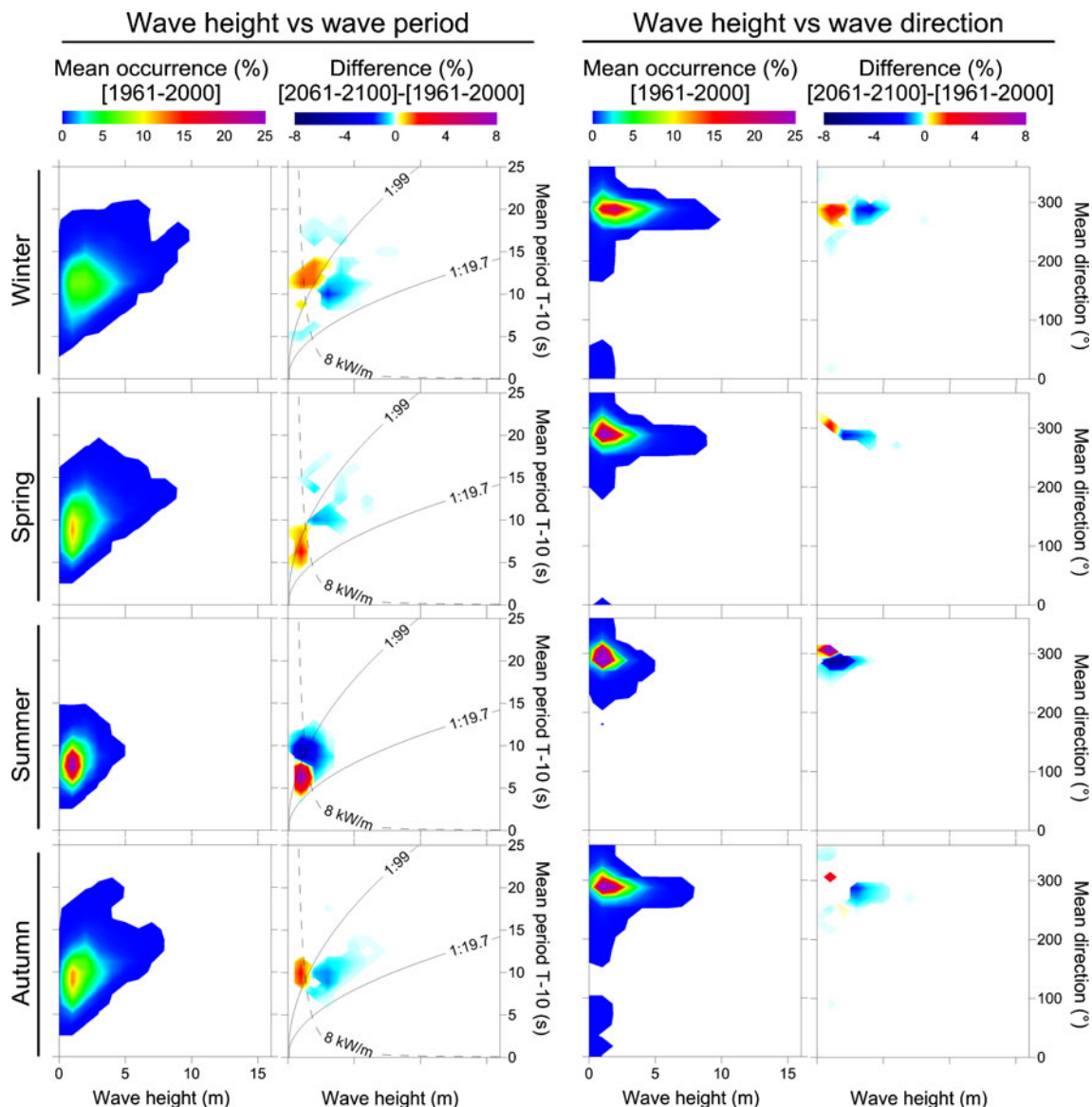


Fig. 11 Bivariate diagrams of corrected wave conditions at the coastal Biscarrosse buoy (26 m depth) for the present REF scenario (1961–2000) and bivariate diagrams of changes between wave conditions of the future A2 scenario (2061–2100) and the present REF scenario (1961–2000). Only changes significant at

more than 95 % (Student's *T* test) are plotted. *Plain lines* indicate the median and the Pierson–Moskovitz steepness, and *dotted line* indicates the median energy flux, calculated from the REF dataset

intermediate waves are less frequent. Summer presents large changes, with a decrease of energetic wave and an increase of non-energetic wave occurrence. Spring and autumn exhibit a decrease of energetic wave and an increase of non-energetic wave occurrence. Wave direction changes are less pronounced than at the offshore buoy. During winter, the previously identified clockwise shift of large waves is not present. During summer, we find the same clockwise shift of wave directions as at the Biscay buoy. However, the direction range being smaller, the wave density increases between 300° and 320° (300–360° at the Biscay buoy) and decreases between 270° and 300° (250–310° at the Biscay buoy), leading to a smaller shift of wave directions.

To summarize, in intermediate to shallow water depths, refraction processes reduce the wave direction shifts, especially for largest waves (winter large swell clockwise shift). The strong refraction of large waves and weak refraction of small waves were also underlined by Bertin et al. (2008). However, the summer clockwise shift of wave directions and the general wave height decrease are still significant in the coastal area.

Those projected wave changes could induce changes of the Biscarrosse sandy beach morphology (bars organization) and in the coastline evolution. For instance, Thiébot et al. (2011) found that different wave directions can generate different geometries and temporal evolutions for a double sandbar system. Regarding longshore sediment transport, Andrade et al. (2007) highlighted a clockwise shift of annual wave directions in future climate (ranging from 5° to 7°) along the Portugal coast that induces an increase of the longshore drift ranging from 5 to 15 %. Along the St Trojan Beach (France), Bertin et al. (2008) also highlighted the importance of the wave angle at breaking: Frontal winter energetic swells are responsible of only 20 % of the net longshore drift, the remaining 80 % being produced by low-energy waves reaching the coast with larger incidence angles.

Along the Aquitanian coast, the wave incidence induces a longshore drift oriented southwards. The present study highlights a general decrease of wave height and a clockwise shift of summer wave direction along the coast. These changes have an opposite action on the longshore sediment flux: The wave height decrease leads to the longshore flux decrease and the wave direction clockwise shift increases the wave incidence angle and thus leads to the longshore flux increase. To assess how the projected wave changes can impact the longshore drift along the Aquitanian coast, we apply a deep-water alongshore sediment flux formula at the Biscarrosse beach (assuming both refraction over shore-parallel contours and no dissipation of

wave energy, for more details, see Ashton et al. (2001)). Located in front of the Biscarrosse buoy and presenting an angle of 8° with the north–south axis, the Biscarrosse beach is representative of the Aquitanian sandy coast. The annual net longshore drift is calculated using the Biscarrosse buoy wave height and direction time series for the present climate (corrected REF dataset from 1961 to 2000) and for the future A2 scenario (corrected A2 dataset from 2061 to 2100). The projected changes in wave conditions for the A2 scenario are leading to a decrease of 10 % of the annual net longshore drift.

When propagating from deep water to intermediate water depths, projected waves present smaller direction changes while wave height and period changes are still significant. Those changes have a noticeable impact on longshore flux magnitude. However, the longshore flux decrease may not induce coastline changes: Further investigation on the spatial variability of longshore sediment flux induced by wave condition changes along the whole Aquitanian coast would be required to identify erosion and accretion areas.

6 Discussion

Focusing on the A2 scenario, we identify several significant wave condition changes in the Bay of Biscay, offshore and along the coast. The investigation of B1 and A1B scenarios (not detailed here) highlights very similar changes, with similar evolution of each wave type. However, we can notice slight differences in amplitude changes: B1 scenario (low emission scenario) exhibits significant changes of smaller amplitude than A1B (medium emission) and A2 (high emission) scenarios, which exhibit a similar amplitude. These differences can be related to associated wind changes: Projected wind changes in A2 and A1B scenarios are very similar, while wind changes in B1 scenario are much smaller. Therefore, the level of GHG emission could modify the amplitude of changes, but not significantly their characteristics. Among the other sources of uncertainties, we took into account the uncertainty related to the interannual natural variability by analysing wave occurrence changes significant at more than 95 % by Student's *T* test. It must be noted that the present study does not examine the uncertainties related to the GCM and to the wave model. Differences in the results of two GCMs simulating a single emission scenario may in fact be larger than the difference between the results from one GCM simulating two different GHG emission scenarios (e.g. Grabemann and Weisse 2008; Debernard and Røed 2008).

To give a first assessment of the uncertainties related to the GCM and the wave model, we compare the present study results to the results underlined in previous studies. Wave height was largely analysed, but no projections of wave period are available within the Bay of Biscay and only one projection of wave direction is available, west of 4° W (Andrade et al. 2007).

Concerning wave height projected changes within the Bay of Biscay, the results are quite different. Studies at global scale and at Ocean Atlantic scale (The WASA Group 1998; Wang et al. 2004; Leake et al. 2007; Wang and Swail 2006; Caires et al. 2006; Mori et al. 2010) give no significant changes or an increase for most of the wave height types, seasons and the emission scenarios. For example, in the most recent study (Mori et al. 2010), annual wave heights exhibit an increase smaller than 5 % in the Bay of Biscay. This is not consistent with the present study results, which show a general decrease of wave heights. Studies at regional scale (Debernard and Røed 2008; Zacharioudaki et al. 2011) show no significant changes or a decrease of wave heights in the Bay of Biscay. In the western part of the Bay of Biscay (west of 2.8° W), Zacharioudaki et al. (2011) underlines a decrease of annual wave heights ranging from −3 to −6 %, with the largest decrease during summer (up to −11 %). Debernard and Røed (2008) also highlighted a significant decrease of summer wave height in the Bay of Biscay. Those two regional studies show changes similar to the present study.

It is also interesting to highlight that the wave height changes projected by previous studies at North Atlantic basin scale are consistent with the ARPEGE-Climat projected wind changes. The studies referred to in the previous paragraph, presenting results in the North Atlantic Ocean, exhibit similar patterns of anomalies: an increase of wave height in the South Western part and in the northeastern part of the North Atlantic Ocean and a decrease in the Central part. These changes have been explained by the projected wind changes (Fig. 7): For the future A2 scenario, wind speed is increasing in the southern part and in the northeastern part of the North Atlantic Ocean and is decreasing in the central part.

Concerning projected wave directions changes, Andrade et al. (2007) project a clockwise shift of annual wave directions along the Portugal coast (5° to 7°) and at the Biscay buoy (between 5° and 10° isocontours). The present study also highlights a clockwise shift, although concerning only summer waves and winter swell.

7 Conclusions

A high spatial resolution dataset of wave conditions in the Bay of Biscay was developed to investigate regional to local changes between present and future wave climate. We applied a dynamical downscaling technique, using the WAVEWATCH III wave model and wind forcing issued from the AGCM ARPEGE-Climat.

Both regional and local wave changes indicate a general decrease of wave height and a clockwise shift of directions during summer. For instance for the A2 scenario averaged over the Bay of Biscay, the significant wave height decreases by 5–11 %, while the mean wave direction increases by 5°. Dynamical downscaling allows a more refined spatial resolution and a better identification of regional scale changes than the previous studies covering the whole North Atlantic Ocean at a much coarser grid resolution. In addition to earlier studies, wave periods and directions were modelled and thoroughly examined. The use of bivariate diagrams allowed to characterize more precisely changes in swell, intermediate waves and wind sea, such as an increase of occurrence and a clockwise shift of winter swell. The amplitude of these changes is larger for higher GHG emissions.

The analysis of wind changes shows that the identified wave changes are consistent with the atmospheric circulation evolution. Moreover, comparison of seasonal and wave type changes highlights not only that several factors contribute to the local wave climate but also that the identified wave changes are complex and result from the joint evolution of wind at oceanic, regional and local scales. For instance, the projected clockwise shift of winter swell direction could be explained by the northeastward shift of the strong wind core in the central North Atlantic Ocean. The winter wave height decrease could be related to the decrease of wind speed both in the central part of the North Atlantic and in the Bay of Biscay. During summer, the projected clockwise shift of directions and decrease of wave heights could be explained by the significant reduction of westerly winds. Those strong winds were generating large waves coming from the W direction bin.

Along the coast, wave height decrease is still significant, whereas summer direction shift is reduced and winter swell direction shift disappears. Regarding coastal dynamics, a reduction of the longshore sediment flux of 10 % is projected at the Biscarrosse beach and is mostly induced by the general decrease of wave height.

Acknowledgements This work was completed during a BRGM-CNRM Ph.D., funded by the AXA Research Fund. The authors thank F. Ardhuin for his precious advice on the use of WW3 wave model and for providing his parameterization, the Computing Center of Region Centre for providing access to the Phoebus computing system and Grand Equipement National de Calcul Intensif for the access to the HPC resources of CINES under the allocation 2010-[c2010016403]. The authors gratefully acknowledge R. Pedreros, F. Dupros, F. Boulahya and N. Desramaut (BRGM) for assistance, interesting exchanges and ideas that led to improve this paper.

Open Access This article is distributed under the terms of the Creative Commons Attribution License which permits any use, distribution, and reproduction in any medium, provided the original author(s) and the source are credited.

References

- Andrade C, Pires H, Taborda R, Freitas M (2007) Projecting future changes in wave climate and coastal response in Portugal by the end of the 21st century. *J. Coast Res SI* 50:263–257
- Ardhuin F, Rogers E, Babanin A, Filipot JF, Magne R, Roland A, Westhuysen AVD, Queffelec P, Lefevre JM, Aouf L, Collard F (2010) Semi-empirical dissipation source functions for ocean waves: part I, definition, calibration and validation. *J Phys Oceanogr* 40:1917–1941. doi:10.1175/2010JPO4324.1
- Ashton A, Murray AB, Arnault O (2001) Formation of coastline features by large-scale instabilities induced by high-angle waves. *Nature* 414:296–300. doi:10.1038/35104541
- Bertin X, Castelle B, Chaumillon E, Butel R, Quique R (2008) Estimation and inter-annual variability of the longshore transport at a high-energy dissipative beach : the St Trojan beach, SW Oléron Island, France. *Cont Shelf Res* 28:1316–1332
- Butel R, Dupuis H, Bonneton P (2002) Spatial variability of wave conditions on the French Atlantic coast using in-situ data. *J Coast Res SI* 36:96–108
- Caires S, Swail VR, Wang XL (2006) Projection and analysis of extreme wave climate. *J Climate* 19:5581–5605. doi:10.1175/JCLI3918.1
- Catto J, Shaffrey LC, Hodges KI (2011) Northern Hemisphere extratropical cyclones in a warming climate in the HiGEM high resolution climate model. *J Climate* 24:5336–5352. doi:10.1175/2011JCLI4181.1
- Charles E, Idier D, Thiébot J, Le Cozannet G, Pedreros R, Ardhuin F, Planton S (2012) Present wave climate in the Bay of Biscay: spatiotemporal variability and trends from 1958 to 2001. *JCLI*. doi:10.1175/JCLI-D-11-00086.1
- Christensen J, Hewitson B, Busuioc A, Chen A, Gao X, Held I, Jones R, Kolli R, Kwon WT, Laprise R, Rueda VM, Mearns L, Menendez C, Raisanen J, Rinke, Sarr A, Whetton P (2007) Regional climate projections. In: climate change 2007: the physical science basis. In: Solomon S, Qin D, Manning M, Chen Z, Marquis M, Averyt K, Tignor M, Miller H (eds) Contribution of working group I to the fourth assessment report of the intergovernmental panel on climate change. Cambridge University Press, Cambridge, pp 847–940
- Debernard JB, Røed LP (2008) Future wind, wave and storm surge climate in the Northern Seas: a revisit. *Tellus A* 60(3):427–438. doi:10.1111/j.1600-0870.2008.00312.x
- Déqué M (2007) Frequency of precipitation and temperature extremes over France in an anthropogenic scenario: model results and statistical correction according to observed values. *Glob Planet Change* 57(1–2):16–26. doi:10.1016/j.gloplacha.2006.11.030. Extreme Climatic Events
- Gibelin AL, Déqué M (2003) Anthropogenic climate change over the Mediterranean region simulated by a global variable resolution model. *Clim Dyn* 20:327–339. doi:10.1007/s00382-002-0277-1
- Gjevik B, Krogstad H, Lygre A, Rygg O (1988) Long period swell wave events on the Norwegian Shelf. *J Phys Oceanogr* 18:724–737
- Grabemann I, Weisse R (2008) Climate change impact on extreme wave conditions in the North Sea: an ensemble study. *Ocean Dyn* 58:199–212. doi:10.1007/s10236-008-0141-x
- Hanley K, Belcher S, Sullivan P (2010) A global climatology of wind-wave interaction. *J Phys Oceanogr* 40:1263–1282
- Hemer M, McInnes K, Ranasinghe R (2012) Climate and variability bias adjustment of climate model-derived winds for a southeast Australian dynamical wave model. *Ocean Dyn* 62(1):87–104. doi:10.1007/s10236-011-0486-4
- Le Cozannet G, Lecacheux S, Delvallée E, Desramaut N, Oliveros C, Pedreros R (2010) Teleconnection pattern influence in the Bay of Biscay. *J Climate*. doi:10.1175/2010JCLI3589.1
- Leake J, Wolf J, Lowe J, Stansby P, Jacob G, Nicholls R, Mokrech M, Nicholson-Cole S, Walkden M, Watkinson A, Hanson S (2007) Predicted wave climate for the UK: towards an integrated model of coastal impacts of climate change. In: Proceeding of the Tenth International Conference on Estuarine and Coastal Modeling Congress 2007, ASCE, pp 393–406. doi:10.1061/40990(324)24
- Lionello P, Cogo S, Galati M, Sanna A (2008) The Mediterranean surface wave climate inferred from future scenario simulations. *Glob Planet Change* 63:152–162
- Mori N, Yasuda T, Mase H, Tom T, Oku Y (2010) Projection of extreme wave climate change under global warming. *Hydrol Res Lett* 4:15–19
- Reichle RH, Koster RD (2004) Bias reduction in short records of satellite soil moisture. *GRL* 31. doi:10.1029/2004GL020938
- Semedo A, Sušelj K, Rutgersson A, Sterl A (2011) A global view on the wind sea and swell climate and variability from era-40. *J Climate* 24:1461–1479. doi:10.1175/2010JCLI3718.1
- The WASA Group (1998) Changing waves and storms in the northeast Atlantic? *Bull Am Meteorol Soc* 79:741–760. doi:10.1175/1520-0477(1998)079<0741:CWASIT>2.0.CO;2
- Thiébot J, Idier D, Garnier R, Falqués A, Ruessink B (2011) The influence of wave direction on the morphological response of a double sandbar system. *Cont Shelf Res* 32:71–85. doi:10.1016/j.csr.2011.10.014
- Tolman HL (2009) User manual and system documentation of wavewatch III version 3.14. Technical Note 276, NOAA/NWS/NCEP/MMAB
- Uppala SM, Kållberg PW, Simmons AJ, Andrae U, da Costa Bechtold V, Fiorino M, Gibson JK, Haseler J, Hernandez A, Kelly GA, Li X, Onogi K, Saarinen S, Sokka N, Allan RP, Andersson E, Arpe K, Balmaseda MA, Beljaars ACM, van de Berg L, Bidlot J, Bormann N, Caires S, Chevallier F, Dethof A, Dragosavac M, Fisher M, Fuentes M, Hagemann S, Hölm E, Hoskins BJ, Isaksen L, Janssen PAEM, Jenne

- R, McNally AP, Mahfouf JF, Morcrette JJ, Rayner NA, Saunders RW, Simon P, Sterl A, Trenberth KE, Untch A, Vasiljevic D, Viterbo P, Woollen J (2005) The ERA-40 re-analysis. *Quart J R Meteor Soc* 131:2961–3012. doi:[10.1256/qj.04.176](https://doi.org/10.1256/qj.04.176)
- Wang XL, Swail VR (2006) Climate change signal and uncertainty in projections of ocean wave heights. *Clim Dyn* 26:109–126. doi:[10.1007/s00382-005-0080-x](https://doi.org/10.1007/s00382-005-0080-x)
- Wang XL, Zwiers FW, Swail VR (2004) North Atlantic Ocean wave climate change scenarios for the twenty-first century. *J Climate* 17:2368–2383. doi:[10.1175/1520-0442\(2004\)017;2368:NAOWCC;2.0.CO;2](https://doi.org/10.1175/1520-0442(2004)017;2368:NAOWCC;2.0.CO;2)
- Wang XL, Swail VR, Cox A (2010) Dynamical versus statistical downscaling methods for ocean wave heights. *Int J Climatol* 30(3):317–332. doi:[10.1002/joc.1899](https://doi.org/10.1002/joc.1899)
- Wood AW, Maurer EP, Kumar A, Lettenmaier DP (2002) Long-range experimental hydrologic forecasting for the eastern United States. *JGR* 107(D20). doi:[10.1029/2001JD000659](https://doi.org/10.1029/2001JD000659)
- Yin JH (2005) A consistent poleward shift of the storm tracks in simulations of 21st century climate. *Geophys Res Lett* 32(L18701). doi:[10.1029/2005GL023684](https://doi.org/10.1029/2005GL023684)
- Zacharioudaki A, Pan S, Simmonds D, Magar V, Reeve DE (2011) Future wave climate over the west-European shelf seas. *Ocean Dyn* 61:807–827. doi:[10.1007/s10236-011-0395-6](https://doi.org/10.1007/s10236-011-0395-6)